Catalytic Single Particle Nano-impacts: Theory and Experiment. Poly(vinylferrocene) Modified Graphene Nanoplatelet Mediated L-Cysteine Oxidation

Qianqi Lin,[§] Chuhong Lin,[§] Haoyu Wu, Christopher Batchelor-McAuley, Richard G. Compton*

Department of Chemistry, Physical and Theoretical Chemistry Laboratory, Oxford University, South Parks Road, Oxford OX1 3QZ, U.K.

[§] Both authors contributed equally to this paper

[*]To whom correspondence should be addressed

Email: richard.compton@chem.ox.ac.uk

Phone: +44 (0) 1865 275957 Fax: +44 (0) 1865 275410

Abstract

The theory of catalytic nano-impacts is developed specifically for the case of a single particle in contact with an electrode for a short period of time in which it mediates electron transfer to or from a species in homogeneous solution. The theory is applied to impacts of chemically modified graphene nanoplatelets in which the immobilized ferrocene/ferrocenium couple is used to mediate the oxidation of L-cysteine in aqueous solution. Theory and experiment are in good agreement and the catalytic rate constant is found to be 2.4 ± 1.2 $M^{-1}s^{-1}$.

1 Introduction

As a powerful electroanalytical method, the nano-impacts technique (also called "single nanoparticle collisions") has developed rapidly in the recent decades.[1-4] The term "nano-impacts" refers to the phenomenon in which a nanoparticle (NP) in solution by virtue of its Brownian motion strikes an inert electrode, where current signals can be recorded due to either the direct oxidation/reduction of the NP itself or to a redox reaction involving solution phase species mediated by the NP.[1-2] In the former case, NPs are consumed after colliding on the supporting electrode, while in the latter the NPs persist as the electrochemical reaction only takes place on the surface of the NPs. The nano-impacts method provides useful information about the NPs, such as their size, concentration and state of agglomeration.[5-9] The reaction rate constants, for both electrochemical electron transfer and chemical catalysis, can also be detected *via* nano-impacts. [10-14]

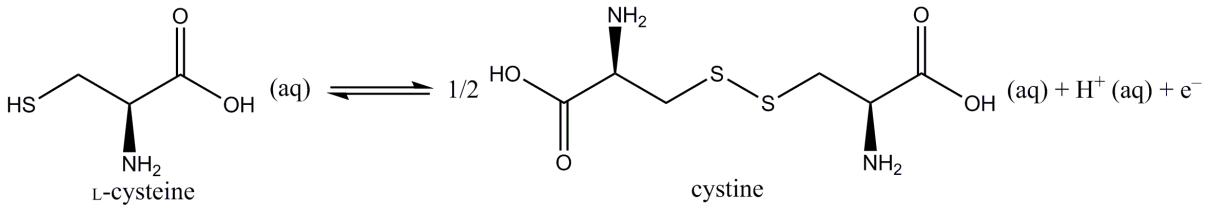

L-cysteine cystine

Scheme 1 Oxidation of L-cysteine to produce cystine.

Ferrocene and its derivatives are widely applied as catalysts in biochemistry and energy technology, since they show rapid electron transfer reactions and so can be used to mediate electron transfer with species which otherwise show slow electron transfer, such as ascorbic acid,[15] sodium peroxide,[16] and sulphide and thiol species.[17-18] In order to observe mediated redox reaction *via* nano-impacts, ferrocene can be modified onto the graphene nanoplatelets (GNPs)[19-20] and dispersed in an aqueous solution with the electroactive species. Herein, poly(vinylferrocene) as a polymeric form of ferrocene is used in order to introduce a high number of catalytic centres. During an impact with an electrode, each single GNP

temporarily acts as an individual tiny electrode and adopts the potential applied.[9] When the potential becomes more positive than that required for ferrocene oxidation, an electrochemical reaction takes place on the GNP. The formed adsorption phase ferrocenium can then bring about mediated electron transfer to solution phase species. Note that the use of individual GNPs circumvents the non-ideal voltammetry[6, 21-24] of large ensembles of particles measured at macro- and microelectrodes, and so provides a more reliable route to measure electron transfer kinetics and mechanisms.[20] In this work L-cysteine, an amino acid with a thiol group (Scheme 1),[18] is employed as the electroactive species under observation. We demonstrate the use of poly(vinylferrocene) modified graphene nanoplatelets (PVFc-GNP) as a mediator for the oxidation of L-cysteine in aqueous solutions and develop the theory of catalytic single particle nano-impacts. The kinetics and mechanism of the catalysis is then assessed synergising both experiment and theory.

2 Theory and Simulation

The simulation model for the mediated catalytic reaction on the individual GNP is developed in this section.

2.1 Theoretical Model

When the modified GNP impacts on an inert electrode, the mediated reaction takes place on the individual GNP. The impacting GNP is treated as a transient micro-disc electrode and the mediated reaction on the GNP is interpreted by an EC' mechanism, where electron transfer between the adsorbed redox species (E) is followed by a heterogeneous catalytic reaction (C'):

$$A(ads) \rightleftharpoons B(ads) + e^- \qquad (1)$$

$$B(ads) + R(sol) \xrightarrow{k_c} A(ads) + P(sol) \qquad (2)$$

where A and B refer to the adsorbates, R and P are the reactant and the product in the solution. In this work, A is the ferrocene modified on the GNP and R is the cysteine dissolved in the solution.

Assuming the electron transfer kinetics can be described by the Butler-Volmer equation, the reaction rate equations for the adsorbate A and the reactant R can be expressed as:

$$\frac{\partial \Gamma_A}{\partial t} = -k_0 \exp\left(\frac{\beta F}{RT}\left(E - E^{o}_{f,\,(A(ads)/B(ads))}\right)\right)\Gamma_A + k_0 \exp\left(-\frac{\alpha F}{RT}\left(E - E^{o}_{f,\,(A(ads)/B(ads))}\right)\right) \left(\Gamma_{max} - \Gamma_A\right) + k_{cat}\left(\Gamma_{max} - \Gamma_A\right) c_{R(surf)} \quad (3)$$

$$D_R \left.\frac{\partial c_R}{\partial z}\right|_{surf} = -k_c \left(\Gamma_{max} - \Gamma_A\right) c_{R(surf)} \quad (4)$$

where Γ_A is the surface coverage of the adsorbate A (mol m^{-2}), k_0 is the standard electrochemical rate constant of Eqn.(1) (s^{-1}), α and β are the transfer coefficients in the Butler-Volmer equation[25-26], E is the potential applied on the electrode (V), $E^{o}_{f,\,(A(ads)/B(ads))}$ is the formal potential (V) for the redox couple A(ads)/B(ads) defined under the condition $\Gamma_A = \Gamma_B$, F is the Faraday constant (96485 C mol^{-1}), R is the gas constant (8.314 J mol^{-1} K^{-1}), T is the absolute temperature (K), k_c is the catalytic rate constant of Eqn.(2) (M^{-1} s^{-1}), $c_{R(surf)}$ is the surface concentration of the reactant R (mol m^{-3}), D_R is the diffusion coefficient of R (m^2 s^{-1}), and z is the coordinate perpendicular to the electrode surface (m). As the maximum adsorption of A, Γ_{max}, on the electrode surface is a constant, the surface coverage of B always equals $\Gamma_{max}-\Gamma_A$. Since the catalytic step is assumed irreversible, the concentration of P is not involved in the simulation.

For the present, we assume the impact occurs for enough time to undertake a voltammetric sweep. For convenience, the overpotential η (V), equal to $E - E^{o}_{f,\,(A(ads)/B(ads))}$, is

applied in the simulation. In cyclic voltammetry, when the potential window is [η_{ini}, η_{rev}] (for the ferrocene/ferrocenium redox reaction, $\eta_{ini} < \eta_{rev}$), the overpotential η (V) is a function of the time t (s) and the scan rate v (V s^{-1}):

$$\eta = \begin{cases} \eta_{ini} + vt & t \le \dfrac{\eta_{rev} - \eta_{ini}}{v} \\ \eta_{rev} + v\left(t - \dfrac{\eta_{rev} - \eta_{ini}}{v} \right) & t > \dfrac{\eta_{rev} - \eta_{ini}}{v} \end{cases} \quad (5)$$

Note that in the experiments discussed below a large overpotential is applied to establish a steady-state current.

The current I (A) is generated only from Eqn.(1), which can be calculated by:

$$I = F\int \left[k_0 \exp\left(\frac{\beta F}{RT}\eta \right)\Gamma_A - k_0 \exp\left(-\frac{\alpha F}{RT}\eta \right)\left(\Gamma_{max} - \Gamma_A\right) \right] dS \quad (6)$$

where S refers to the area of the electrode surface (m^2). The theory developed is general for any disc and the specific application to nano-impacts is considered below.

Migration and convection in our experiment can be neglected, as the solution is assumed to be fully supported by the electrolyte, there is no external force applied to the solution and the experimental time is short enough to avoid natural convection.[27-28] Thus the concentration of R in solution is described by the diffusion equation, Fick's second law:

$$\frac{\partial c_R}{\partial t} = D_R \nabla^2 c_R \quad (7)$$

By solving the partial differential equation (7) combined with the boundary conditions Eqn.(3) and (4), the current on the electrode can be derived.

2.2 Numerical Simulation

The reaction is considered to take place on a microdisc. The latter is illustrated in Figure 1a, where the cylindrical coordinates *z* and *r* represent the directions perpendicular to and radial from the electrode, respectively. Figure 1b shows the calculation grids implemented in the simulation. Expanding grids[29-30] are applied to optimize the computation and all the simulation results presented in this paper are convergent.

The resulting problem was solved numerically by means of the Newton-Raphson method and the alternating direction implicit (ADI) method, the details of which can be found in the literature.[31] The simulation was written in C++ with OpenMP for multithreading, and simulations were performed using an Intel(R) Xeon(R) 3.60G CPU. The runtime varied between approximately 20 minutes per voltammogram.

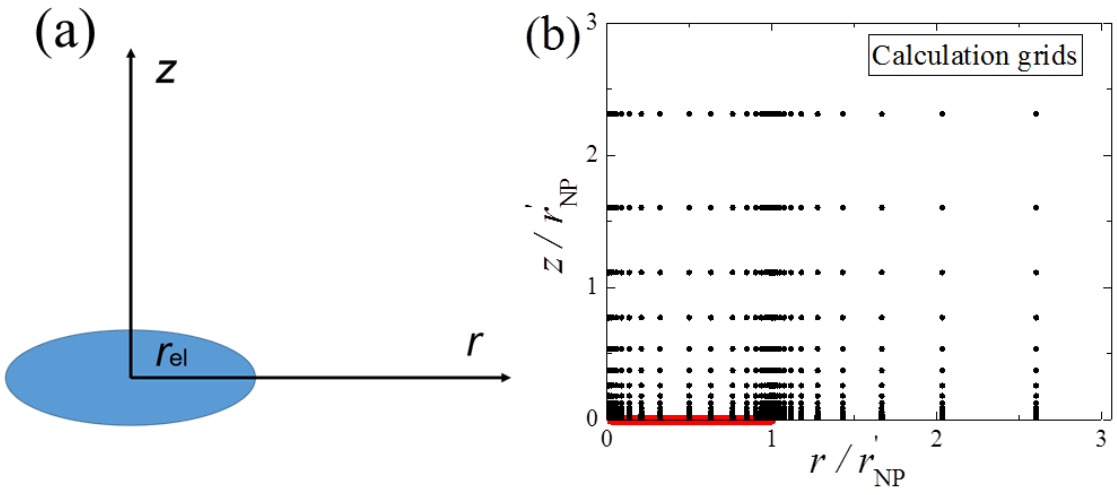

Figure 1 (a) Two-dimensional scheme of the microdisc electrode. (b) Calculation grids applied in the simulation. The red line shows the position of the microdisc electrode.

2.3 Voltammetric Characterisation

The voltammograms of an electron transfer in the simple oxidation of adsorbate A ("E reaction", Figure 2a) and a heterogeneous EC' reaction (Figure 2b) were simulated for various standard electrochemical rate constants, k_0. In the simple E reaction, the maximum surface coverage was selected as 2×10^{-6} mol m^{-2}, the radius of the microdisc electrode as 10

μm, and the scan rate as 0.05 V s^{-1}. As shown in Figure 2a, a peak is generated around the formal potential of the A(ads)/B(ads) redox couple and the current drops to zero at high overpotentials. This wave shape and the decrease to zero current are a consequence of the finite amount of electroactive species on the electrode surface. A decrease in k_0 causes changes in both the adsorption peak height and the peak position. For the EC' reaction, the concentration of R was selected as 1 mM, the catalytic rate constant as 1 M^{-1} s^{-1}, and the diffusion coefficient of R as 1×10^{-9} m^2s^{-1}. The rest of the simulation conditions were the same as those set for the E reaction. Figure 2b shows when the product of the E reaction becomes the mediator of the following catalytic reaction, the current signal is enhanced and the voltammogram shows distinct and different wave shape. The peak vanishes and the current at high overpotentials is not zero but reaches a steady state. The effect of k_0 is reflected on the half-wave potential while the steady-state current is independent of k_0.

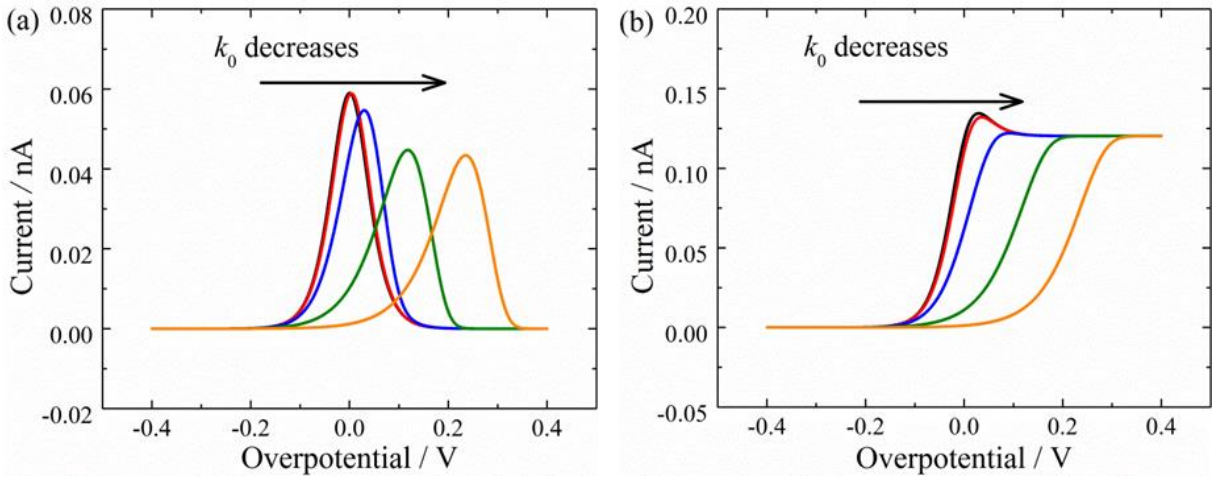

Figure 2 Influence of the electron transfer rate on the cyclic voltammograms. (a) E reaction. (b) EC' mechanism. k_0 applied in the simulation are 100, 10, 1, 0.1, 0.01 s^{-1}, respectively. The rest of the simulation conditions can be found in the text.

For the case of nano-impacts where the entire reaction is confined to an impacting particle, such as a GNP, the tiny size of the latter ensures that the steady-state diffusion of R is rapidly established. The analytical expression of the steady-state current can be derived on the basis of the steady-state approximation. At steady state, the reaction rate of the

intermediate B of Eqns. (1) and (2) should be zero. Given that $\Gamma_B = \Gamma_{max} - \Gamma_A$, the reaction rate of the adsorbate A is zero as well:

$$\frac{\partial \Gamma_A}{\partial t} = -k_0 \exp\left(\frac{\beta F}{RT}\eta\right)\Gamma_A + k_0 \exp\left(-\frac{\alpha F}{RT}\eta\right)\left(\Gamma_{max} - \Gamma_A\right) + k_c\left(\Gamma_{max} - \Gamma_A\right)c_{R(surf)} = 0 \qquad (8)$$

The current density at steady state can be then expressed as:

$$\frac{I}{FS} = k_c\left(\Gamma_{max} - \Gamma_A\right)c_{R(surf)} \qquad (9)$$

At the steady-state, the diffusion on the microelectrode surface can be approximated as linear and the concentration of R, as well as the surface coverage of A, is considered uniform in the radial direction. Therefore, the concentration difference only appears on the direction perpendicular to the electrode surface and the concentration gradient of R at the electrode surface can be calculated by:

$$D_R \left.\frac{\partial c_R}{\partial z}\right|_{surf} = D_R \frac{c_R^* - c_{R(surf)}}{\delta} = k_c\left(\Gamma_{max} - \Gamma_A\right)c_{R(surf)} \qquad (10)$$

where δ is the diffusion layer thickness. For a microdisc electrode, the diffusion layer thickness equals to $\pi r_{el}/4$. The surface coverage of the adsorbate A is zero at steady state. Combining Eqns. (9) with (10) gives the steady-state current for a heterogeneous EC' reaction on a microdisc electrode:

$$I_{ss} = FS\frac{k_c c_R^* \Gamma_{max}}{1 + \frac{\pi k_c \Gamma_{max} r_{el}}{4D_R}} \qquad (11)$$

Therefore, when the steady-state current is known, the catalytic reaction rate constant of the heterogeneous EC' reaction (k_c) can be determined.

It is interesting to note if the catalytic reaction is extremely fast compared to the diffusion process of the reactant R, so that $k_c\Gamma_{max} \geq D_R/\delta$, the steady-state current of the EC' reaction will reach its maximum value:

$$I_{ss,max} = FS\frac{4D_R c_R^*}{\pi r_{el}} \quad (12)$$

where the maximum steady-state current, $I_{ss,max}$, is only limited by the diffusion of the reactant R.

3 Experimental

3.1 Chemical Reagents and Solutions

The graphene nanoplatelets (GNPs, radius of 7.5 μm, thickness of 7 nm, bulk density of 1×10^5 g m^{-3}) were purchased from Strem Chemicals (Newburyport, MA, U.S.).[32] The size of GNPs was confirmed by Scanning Electron Microscopy imaging.[33] The weight of the GNPs is 1.68×10^{12} g mol^{-1}, assuming its density to be the same as that of graphite, 2.26×10^6 g m^{-3}.[34] Note that the bulk density corresponds to the GNPs loose powder but not the actual particles. Poly(vinylferrocene) [PVFc, molecular weight of *ca.* 50,000] was provided by Polyscience Inc. (Warrington, PA, U.S.). All other chemicals were purchased from Sigma-Aldrich (St Louis, MO, U.S.) and used as received. The structure of L-cysteine is depicted in Scheme 1, along with the oxidation product, cystine. pH 7 buffer aqueous solution was prepared using 0.1 M potassium phosphate mono- and dibasic, with 0.1 M KCl as supporting electrolyte. pH 7 buffer was used to mimic the biological environment. Where aqueous solution is mentioned, it is prepared using deionised water with resistivity not less than 18.2 MΩ cm at 298 K (Millipore, Billerica, MA, U.S.).

3.2 Preparation of PVFc Modified GNPs

PVFc modified GNPs (PVFc-GNPs) were prepared as following. Two stock solutions were made fresh daily: 2.1 mg of PVFc in 5 mL of dichloromethane (DCM), and 7.0 mg of GNPs in another 25 mL of DCM. The latter was sonicated (FB15050, Fisher Scientific, 50/60 Hz, 80 W, Germany) for 10 min to allow an evenly distributed suspension. Amount of 1 mL of each stock solution were mixed in a sample vial, and left in a desiccator for 30 min to evaporate the solvent. Only PVFc-GNPs at the bottom of the vial was transferred for further reactions, leaving the excess PVFc remain in the vial walls during evaporation of the solvent.

3.3 Electrochemical Apparatus

A standard three electrode cell was employed to conduct all the electrochemical experiments. An edge-plane pyrolytic graphite (EPPG) electrode (radius 2.0 mm) was used for preliminary voltammetric measurements, while a carbon fibre micro wire electrode (radius 3.5 μm and length 1 mm) was used for the nano-impact measurements, both acting as the working electrode. The in-house EPPG was fabricated using highly ordered pyrolytic graphite (Le Carbone, Sussex, U.K.). The carbon fibre micro wire electrodes were prepared following the method developed by Ellison *et al*.[35] A saturated calomel electrode (SCE, ALS distributed by BASi, Tokyo, Japan) and a platinum wire (99.99% GoodFellow, Cambridge, U.K.) were used as the reference and counter electrode respectively. Voltammetry was recorded using a μAutolab III potentiostat (Autolab, Utrecht, Netherlands) and nano-impact chronoamperometry was conducted using an in-house built low noise potentiostat.[36] All the experiments were completed in a Faraday cage thermostated at 25 ± 1 ^{o}C.

3.4 Experimental Procedures

For cyclic voltammetry, the EPPG electrode was cleaned by polishing in an alumina slurry of decreasing particle size (1.0-0.05 μm, Buehler, IL, U.S.). A cyclic voltammogram in a blank pH 7 aqueous solution was run with 0.1 M KCl to confirm the cleanliness of the electrode. After the EPPG electrode was rinsed and nitrogen (N_2) blown dried, it was transferred to a filter paper (70 mm, Fisherband, Loughborough, U.K.) with the prepared PVFc-GNPs. The particles were abrasively modified onto the electrode surface for at least 100 cycles of figure of eight. After the electrode modifications, a cyclic voltammogram was recorded in 25 mL of either blank or 10 mM L-cysteine pH 7 aqueous solution with 0.1 M KCl at a scan rate of 50 mV s^{-1}.

For nano-impact chronoamperometry, the prepared PVFc-GNPs were suspended in 5 mL of various concentrations of a L-cysteine pH 7 aqueous solution supported with 0.1 M KCl. The concentration of the GNPs was *ca.* 3×10^{-14} M.[20, 37] The mixture was sonicated to achieve a good suspension, and bubbled with N_2 to remove the dissolved oxygen. Nano-impact chronoamperometry was run at the same time as degassing. As a control experiment, another chronoamperometry was run while degassing in the same electrolytic solution but with the absence of the GNPs. Figure SI1 in Supporting Information shows that degassing may cause some small noise to the baseline, but does not generate any current spikes interfering the nano-impacts study. Two potentials, +0.20 and +1.00 V, were applied to the electrode for 20 s to generate a chronoamperogram.

4 Results and Discussion

In this section, we report first how the PVFc-GNPs were immobilised on a macro-size edge-plane pyrolytic graphite (EPPG) electrode. The corresponding cyclic voltammetry is then

discussed, in order to determine the overpotential required to fully drive the reaction. Second, the PVFc-GNPs were dispersed on the electrolytic solution with different concentrations of L-cysteine. The nano-impacts of individual PVFc-GNP at a micro-size carbon fibre electrode were studied chronoamperometrically. Finally, the experimental results were simulated using the theoretical model, allowing inference of the mechanism and measurement of the catalytic rate constant.

4.1 Cyclic Voltammetry

The cyclic voltammetry of PVFc-GNPs was first studied by abrasively modifying the particles onto an EPPG electrode surface. As more fully described in the Experimental section, following the synthesis of PVFc-GNPs, the particles were placed on a filter paper for the abrasive modification of the electrode. The modified electrode was then transferred to 25 mL of pH 7 aqueous solution supported with 0.1 M KCl. Cyclic voltammetry was run from 0 to +0.70 V (*vs.* SCE) and reversed to 0 V at a scan rate of 50 mV s^{-1} (Figure 3c). Another unmodified electrode was immersed in the same electrolytic solution to run the voltammogram (Figure 3d). Comparison of the lines shows that an oxidative response can be observed at *ca.* +0.52 V with the peak height of *ca.* 2.6 μA (Figure 3, inlay), which corresponds to the oxidation of the adsorbed ferrocene moiety to the ferrocenium cation:

$$Cp_2Fe\,(ads) + Cl^- \rightleftharpoons Cp_2Fe^+Cl^-(ads) + e^- \qquad (13)$$

The inlay of Figure 3 shows a reductive response as a broad peak at *ca.* +0.32 V with the height of *ca.* 0.6 μA. The back peak is less well-defined as the forward peak, as a result of the ion-pairing between the ferrocenium cation and the chloride anion from the supporting electrolyte. Such coordination stabilises the ferrocenium cation and hence its reduction becomes less favourable (the so-called 'square scheme')[38-39]. In contrast, PVFc-GNPs

supported with $NaClO_4$ shows a higher redox signal commenced at lower potential (Supporting Information, Figure SI2). However, 10 mM L-cysteine was observed to precipitate in 25 mL of pH 7 aqueous solution supported with 0.1 M $NaClO_4$, precluding its use in the mediated oxidation of L-cysteine. KCl was the optimal electrolyte due to the higher solubility of L-cysteine.

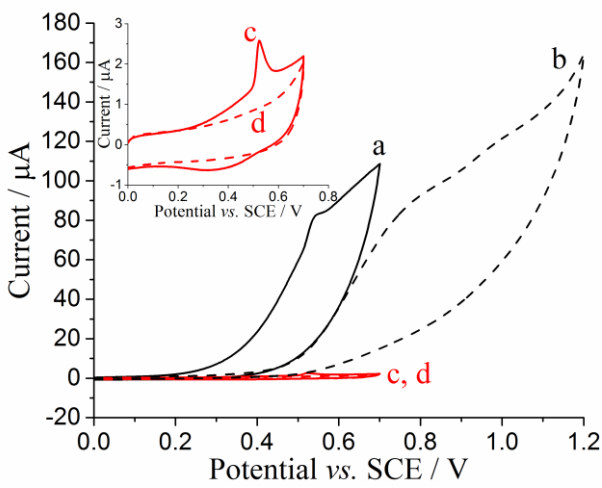

Figure 3 Voltammogram in a N_2 degassed pH 7 aqueous solution supported with 0.1 M KCl at PVFc-GNPs modified EPPG electrodes *via* abrasive modification (a and c), and at unmodified EPPG electrodes (b and d). 10 mM L-cysteine is presence in a and b. L-cysteine is absence in c and d. Scan rate = 50 mV s^{-1}.

The investigation next examined the cyclic voltammetry of L-cysteine containing solutions at EPPG electrode. An unmodified electrode was investigated in 25 mL of 10 mM L-cysteine pH 7 aqueous solution supported with 0.1 M KCl to record the voltammogram in a wide potential window between 0 and +1.20 V (*vs.* SCE). Figure 3b shows a poorly defined oxidative response at *ca.* +0.80 V, which is in a good agreement with the reported value, +0.81 V, for the *direct* oxidation of L-cysteine in a pH 7 buffer solution.[18] In contrast when the modified electrode was transferred to the same 10 mM L-cysteine solution to run the voltammetry (Figure 3a) an oxidative response was observed at *ca.* +0.54 V, close to the oxidation potential of the ferrocene moiety. This can be ascribed to the oxidation of L-

cysteine mediated by the ferrocenium cation. The following EC' catalytic mechanism is proposed:

$$Cp_2Fe(ads) \overset{k_0}{\rightleftharpoons} Cp_2Fe^+(ads) + e^- \qquad (14)$$

$$Cp_2Fe^+(ads) + \text{L-cysteine(sol)} \xrightarrow{k_c} Cp_2Fe(ads) + \text{product(sol)} \qquad (15)$$

where the Cp_2Fe/Cp_2Fe^+ couple serves as the catalyst for the oxidation of L-cysteine, k_0 is the standard electrochemical rate constant of the Cp_2Fe/Cp_2Fe^+ couple at the GNPs surface, and k_c is the heterogeneous rate constant of reaction (15). After the ferrocene moiety is oxidised at the GNPs surface, an electron is transferred from L-cysteine in solution to the ferrocenium cation adsorbed at the GNPs. Cystine is generated at a much lower potential (Figure 3a) compared to the direct oxidation of L-cysteine (Figure 3b). The outcome of the catalysis shows an oxidative signal, as well as a relative loss of chemical reversibility due to the tiny concentration of the Cp_2Fe/Cp_2Fe^+ couple in comparison with L-cysteine.[40] After the conversion of Cp_2Fe to Cp_2Fe^+, the latter participates in the catalytic cycle. Since little Cp_2Fe^+ is left to reproduce Cp_2Fe, there is a negligible reductive back peak in Figure 3a.

Although the catalytic response is qualitatively observed on the PVFc-GNP modified EPPG electrode in Figure 3, the voltammetric signal cannot be applied to determine the kinetic parameters in the catalytic oxidation reaction of L-cysteine. Given that the mass transport to the EPPG electrode modified with a porous GNP layer is uncertain, it is difficult to interpret the scan rate dependence of the signal. Moreover, the modification of particles on the electrode can lead to agglomeration and/or aggregation,[6, 23-24] which again mitigates against modelling and quantitative analysis. Therefore, in order to correctly understand the kinetics of the electrocatalytic reaction, the direct measurement of the reaction signal on the individual particles is needed.

4.2 Nano-impact Chronoamperometry

Having evidenced that PVFc-GNPs can mediate the oxidation of L-cysteine, the work turns to study the nano-impacts of PVFc-GNPs in L-cysteine containing solutions at carbon fibre micro wire electrodes. According to the results in the cyclic voltammetry at the PVFc-GNPs modifed EPPG electrodes, the mediated oxidation of L-cysteine is expected to commence when the potential applied to the electrode is at least *ca.* +0.54 V (*vs*. SCE).

The electrode was potentiostatted at +1.00 V (*vs*. SCE) to allow a large overpotential[20] to fully drive the reactions (14) and (15). As discussed in the context of Figure 2, at high overpotentials the oxidation of L-cysteine at an individual PVFc-GNP can reach a steady state, allowing the characterisation of the catalytic mechanism and kinetics. The prepared PVFc-GNPs were first suspended in 5 mL of pH 7 / 0.1 M KCl aqueous solution with the absence of L-cysteine. A chronoamperometry was run using a carbon fibre microwire electrode. When there is no L-cysteine in the solution (Figure 4a), nano-impact spikes of PVFc-GNPs were observed. The charge passed per spike can be estimated by taking the integrated area under the individual spike, with the average value denoted as $\bar{Q}$. For the absence of L-cysteine, $\bar{Q}$ is $6\ ^{+8}_{-6}$ pC. The PVFc-GNPs was then suspended in 5 mL of 20 mM L-cysteine / 0.1M KCl solution. Figure 4e shows the nano-impacts signals are significantly enhanced, with the value for $\bar{Q}$ as 180 ± 172 pC. Further, the experiment was repeated for various concentrations of L-cysteine, 5 mM (Figure 4b), 10 mM (Figure 4c) and 15 mM (Figure 4d). The corresponding $\bar{Q}$ for the three concentrations is $13\ ^{+45}_{-13}$ pc, 62 ± 31 pC and 131 ± 105 pc, respectively. The variation is shown in Figure 5 (squares), where $\bar{Q}$ is plotted against the concentration of L-cysteine ($c^*_{\text{L-cysteine}}$).

In order to demonstrate the switch on/off of the reactions (2) and (3) corresponding to the oxidation of the ferrocene moieties, or not, a potential +0.20 V was applied to the

electrode to run the chronoamperometry of PVFc-GNPs in the same series of solutions varying the concentration of L-cysteine. The corresponding $\bar{Q}$ is plotted against $c^*_{\text{L-cysteine}}$, as shown as dots in Figure 5. Despite of the change in $c^*_{\text{L-cysteine}}$, $\bar{Q}$ remains constant at 2 ± 1 pC.

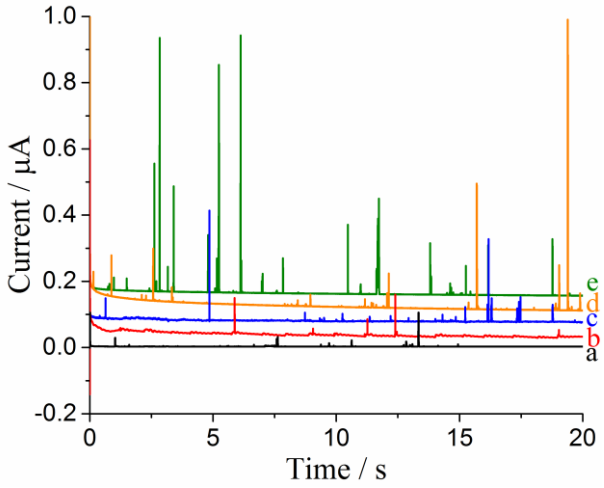

Figure 4 Nano-impacts chronoamperograms of 3 × 10^{-14} M GNPs suspension at carbon fibre micro wire electrodes potentiostatted at +1.00 V (*vs*. SCE), in a N_2 degassed pH 7 aqueous solution supported with 0.1 M KCl. Various concentration of L-cysteine is used: 0 mM (a), 5 mM (b), 10 mM (c), 15 mM (d), and 20 mM (e). Baselines are shifted vertically for clarity.

There are two possible physical origins of the charge transfer involved in the nano-impacts: a catalytic response following the Faradaic process as demonstrated above, or a capacitative response.[20, 36-37] In the former case, Faradaic charge transfer first takes place between PVFc and the electrode [Eqn. (14)], the resulting ferrocenium cation then undergoes further electron transfer with L-cysteine in the solution to produce cystine [Eqn. (15)]. The overall charge transfer should relate to the concentration of L-cysteine. Herein a threshold potential is required to drive the redox reaction (14) and the subsequent catalytic reaction (15). In the latter case, a nanoparticle becomes charged upon collision with the potentiostatted electrode. To maintain the charge neutrality, electrons move in or out of the electrode when the applied potential deviates from the potential of zero charge (PZC). The charge transfer should be independent on the reactions. Figure 5 shows at +0.20 V (*vs*. SCE), $\bar{Q}$ remains unchanged at different $c^*_{\text{L-cysteine}}$, hence only capacitative impacts likely occur. At +1.00 V (*vs*. SCE), $\bar{Q}$ increases with $c^*_{\text{L-cysteine}}$, inferring impacts arise due to the catalysis of L-cysteine

following the Faradaic electron transfer between PVFc and the GNPs [reactions (14) and (15)].

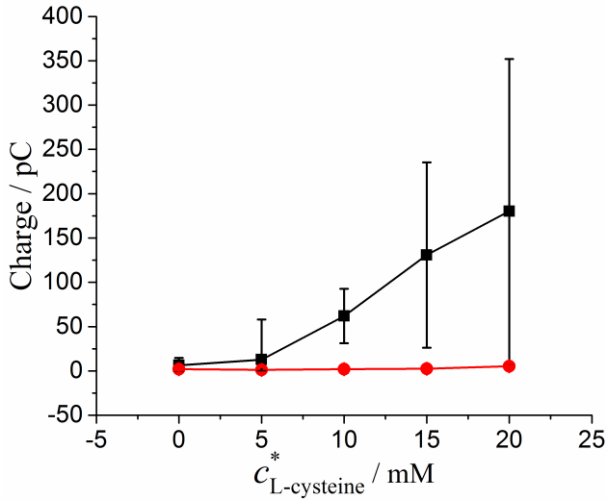

Figure 5 The average charge ($\bar{Q}$) passed per nano-impacts spike dependence of L-cysteine concentration ($c^*_{\text{L-cysteine}}$), at +1.00 V (squares) and +0.20 V (dots) *vs*. SCE. The error bars are obtained from SD/$(n')^{1/2}$, where SD is the standard deviation and n' is the number of spikes.

4.3 Simulation of Nano-impacts Spikes: Derivation of Catalytic Rate Constant

As discussed in the context of Eqn.(11), a steady-state current can be used to infer kinetic information for the catalytic reaction of L-cysteine on PVFc-GNPs. However, due to the short residence time of the colloid, direct measurement of the steady-state current (I_{ss}) on an individual GNP is not easy.[41] Instead, an average I_{ss} is obtained implicitly from the reaction charge (Q) and duration (t_{impact}) per nano-impacts spike, *via* $I_{ss} = Q / t_{\text{impact}}$. Q and t_{impact} are collected at high overpotentials where the steady-state current is reached. After analysis of the nano-impacts spikes, the experimental I_{ss} is plotted as a function of $c^*_{\text{L-cysteine}}$ varying from 5 mM to 20 mM (Figure 6, black squares with error bars). The experimental I_{ss} is shown to be proportional with $c^*_{\text{L-cysteine}}$, which consistent with Eqn.(11). This supports the choice of mechanism used in analysing the experimental data.

In Figure 6, the red and blue lines are the theoretical prediction for the largest and the lowest steady-state currents, according to the distribution of the experimental value of I_{ss}. The

gradient of the two lines is used to derive the boundary of the catalytic rate constant (k_c). A range of k_c can hence be determined by considering the distribution of the experimental I_{ss}. According to Eqn.(11), after plotting I_{ss} against $c^*_{\text{L-cysteine}}$, the gradient can be expressed as:

$$\frac{dI_{ss}}{dc^*_{\text{L-cysteine}}} = FS\frac{k_c\Gamma_{max}}{1+\frac{\pi k_c\Gamma_{max}r_{el}}{4D_{\text{L-cysteine}}}} \qquad (16)$$

where the maximum surface coverage (Γ_{max}) and the standard electrochemical rate constant (k_0) were measured from the redox reaction of PVFc/PVFc$^+$ in the previous work, as *ca.* 2 × 10^{-6} mol m^{-2} and k_0 is *ca.* 3 s^{-1}, respectively.[42] The diffusion coefficient of L-cysteine ($D_{\text{L-cysteine}}$) was reported as 7.9 × 10^{-10} m^{2}s^{-1}.[43] The radius of GNP (r_{el}) is 7.5 μm. The catalytic rate constant (k_c) can thus be derived from the blue and red line, as 1.3 M^{-1} s^{-1} and 3.6 M^{-1} s^{-1}, respectively. Moreover, the values for k_c are used to simulate the I_{ss} (Figure 6, circles). The simulated results match with the analytical lines, demonstrating the validity of Eqn.(11) in derivation of k_c.

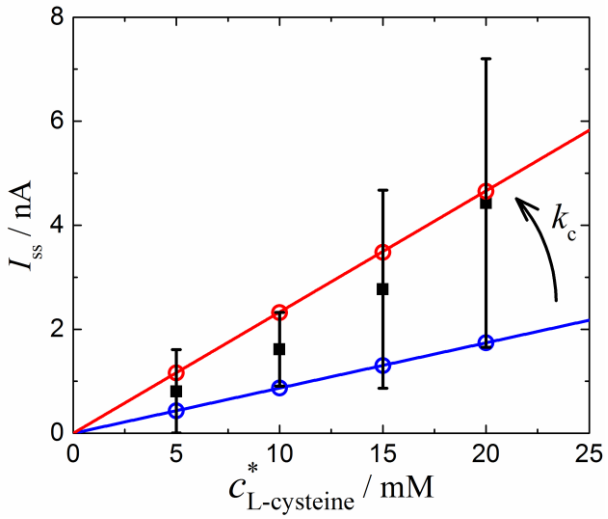

Figure 6 L-cysteine concentration ($c^*_{\text{L-cysteine}}$) variation of the steady-state current (I_{ss}) per nano-impacts spike. Black squares: experimental I_{ss}. The error bars are obtained from SD/(n')$^{1/2}$. Circles: simulated I_{ss}, with catalytic reaction rate (k_c) of 1.3 M^{-1} s^{-1} (red) and 3.6 M^{-1} s^{-1} (blue). Lines: calculated I_{ss} from Eqn.(11) to fit experimental I_{ss} within its error bars. The gradient change between the red and blue lines corresponds to a range of k_c. In the

simulation, parameters used are Γ_{max} = 2 × 10^{-6} mol m^{-2}, k_0 = 2 m s^{-1}, r_{el} = 7.5 μm and $D_{L\text{-}cysteine}$ = 7.9×10^{-10} m^2s^{-1}.

5 Conclusions

The theory for catalytic nano-impacts has been developed for the case where the impacting particle mediates electron transfer to a solution phase species bringing about chemical reactions. For tiny particle, the fast diffusion of the reactant to the surface can establish a steady-state current which reflects the concentration of the target. The theory has been applied to the oxidation of cysteine mediated with ferrocene modified graphene nanoplatelets and a rate constant estimated.

Supporting Information

Further information relating to chronoamperometry of degassing the electrolyte solution and the choice of supporting electrolyte. This material is available free of charge on the ACS Publications website.

Acknowledgements

The research is sponsored by the funding from the European Research Council under the European Union Seventh Framework Programme (FP/2007-2013) / ERC Grant Agreement n. [320403].

References

(1) Bard, A. J.; Zhou, H.; Kwon, S. J. Electrochemistry of Single Nanoparticles via Electrocatalytic Amplification. *Isr. J. Chem.* **2010,** *50*, 267-276.
(2) Cheng, W.; Compton, R. G. Electrochemical Detection of Nanoparticles by 'Nano-Impact' Methods. *TrAC, Trends Anal. Chem.* **2014,** *58*, 79-89.
(3) Pumera, M. Impact Electrochemistry: Measuring Individual Nanoparticles. *ACS Nano* **2014,** *8*, 7555-7558.

(4) Rees, N. V. Electrochemical Insight from Nanoparticle Collisions with Electrodes: A Mini-Review. *Electrochem. Commun.* **2014,** *43*, 83-86.
(5) Xiao, X.; Fan, F.-R. F.; Zhou, J.; Bard, A. J. Current Transients in Single Nanoparticle Collision Events. *J. Am. Chem. Soc.* **2008,** *130*, 16669-16677.
(6) Toh, H. S.; Batchelor-McAuley, C.; Tschulik, K.; Uhlemann, M.; Crossley, A.; Compton, R. G. The Anodic Stripping Voltammetry of Nanoparticles: Electrochemical Evidence for the Surface Agglomeration of Silver Nanoparticles. *Nanoscale* **2013,** *5*, 4884-4893.
(7) Zhou, Y. G.; Rees, N. V.; Compton, R. G. The Electrochemical Detection and Characterization of Silver Nanoparticles in Aqueous Solution. *Angew. Chem. Int. Ed.* **2011,** *50*, 4219-4221.
(8) Plowman, B. J.; Young, N. P.; Batchelor-McAuley, C.; Compton, R. G. Nanorod Aspect Ratios Determined by the Nano-Impact Technique. *Angew. Chem. Int. Ed.* **2016,** *55*, 7002-7005.
(9) Thearle, R. A.; Sofer, Z.; Bouša, D.; Pumera, M. Impact Electrochemistry: Detection of Graphene Nanosheets Labeled with Metal Nanoparticles through Oxygen Reduction Mediation. *ChemPhysChem* **2016,** *17*, 2096-2099.
(10) Cheng, W.; Compton, R. G. Quantifying the Electrocatalytic Turnover of Vitamin B12-Mediated Dehalogenation on Single Soft Nanoparticles. *Angew. Chem. Int. Ed.* **2016,** *55*, 2545-2549.
(11) Li, X.; Batchelor-McAuley, C.; Whitby, S. A. I.; Tschulik, K.; Shao, L.; Compton, R. G. Single Nanoparticle Voltammetry: Contact Modulation of the Mediated Current. *Angew. Chem. Int. Ed.* **2016,** *55*, 4296-4299.
(12) Shimizu, K.; Tschulik, K.; Compton, R. G. Exploring the Mineral-Water Interface: Reduction and Reaction Kinetics of Single Hematite (α-Fe_2O_3) Nanoparticles. *Chem. Sci.* **2016,** *7*, 1408-1414.
(13) Jiao, X.; Lin, C.; Young, N. P.; Batchelor-McAuley, C.; Compton, R. G. Hydrogen Oxidation Reaction on Platinum Nanoparticles: Understanding the Kinetics of Electrocatalytic Reactions via "Nano-Impacts". *J. Phys. Chem. C* **2016,** *120*, 13148-13158.
(14) Lin, Q.; Compton, R. G. Quantifying Adsorption on Single Alumina Particles via Impact Voltammetry and Current Transient Analysis. *J. Phys. Chem. C* **2015,** *119*, 23463-23469.
(15) Casado, C. M.; Cuadrado, I.; Morán, M.; Alonso, B.; Barranco, M.; Losada, J. Cyclic Siloxanes and Silsesquioxanes as Cores and Frameworks for the Construction of Ferrocenyl Dendrimers and Polymers. *Appl. Organomet. Chem.* **1999,** *13*, 245-259.
(16) Yin, W.-W.; Yue, J.-L.; Cao, M.-H.; Liu, W.; Ding, J.-J.; Ding, F.; Sang, L.; Fu, Z.-W. Dual Catalytic Behavior of a Soluble Ferrocene as an Electrocatalyst and in the Electrochemistry for Na-Air Batteries. *J. Mater. Chem. A* **2015,** *3*, 19027-19032.
(17) Lawrence, N. S.; Tustin, G. J.; Faulkner, M.; Jones, T. G. J. Ferrocene Sulfonates as Electrocatalysts for Sulfide Detection. *Electrochim. Acta* **2006,** *52*, 499-503.
(18) Raoof, J. B.; Ojani, R.; Kolbadinezhad, M. Differential Pulse Voltammetry Determination of L-Cysteine with Ferrocene-Modified Carbon Paste Electrode. *B. Chem. Soc. Jpn.* **2005,** *78*, 818-826.
(19) Yang, M.; Batchelor-Mcauley, C.; MoreiraGonçalves, L.; Lima, C. F. R. A. C.; Vyskočil, V.; Tschulik, K.; Compton, R. G. Ferrocene Aryl Derivatives for the Redox Tagging of Graphene Nanoplatelets. *Electroanalysis* **2016,** *28*, 197-202.
(20) Wu, H.; Lin, Q.; Batchelor-McAuley, C.; Compton, R. G. Nanoimpacts Reveal the Electron-Transfer Kinetics of the Ferrocene/Ferrocenium Couple Immobilised on Graphene Nanoplatelets. *ChemElectroChem* **2016**, In press, DOI: 10.1002/celc.201600296.

(21) Stuart, E. J. E.; Tschulik, K.; Batchelor-McAuley, C.; Compton, R. G. Electrochemical Observation of Single Collision Events: Fullerene Nanoparticles. *ACS Nano* **2014,** *8*, 7648-7654.
(22) Zhou, X.; Cheng, W.; Compton, R. G. Contrasts between Single Nanoparticle and Ensemble Electron Transfer: Oxidation and Reduction of DPPH Nanoparticles in Aqueous Media. *ChemElectroChem* **2015,** *2*, 691-699.
(23) Toh, H. S.; Compton, R. G. 'Nano-Impacts': An Electrochemical Technique for Nanoparticle Sizing in Optically Opaque Solutions. *ChemistryOpen* **2015,** *4*, 261-263.
(24) Toh, H. S.; Jurkschat, K.; Compton, R. G. The Influence of the Capping Agent on the Oxidation of Silver Nanoparticles: Nano-Impacts Versus Stripping Voltammetry. *Chem. - Eur. J.* **2015,** *21*, 2998-3004.
(25) Guidelli, R.; Compton, R. G.; Feliu, J. M.; Gileadi, E.; Lipkowski, J.; Schmickler, W.; Trasatti, S. Defining the Transfer Coefficient in Electrochemistry: An Assessment (IUPAC Technical Report). *Pure Appl. Chem.* **2014,** *86*, 245-258.
(26) Guidelli, R.; Compton, R. G.; Feliu, J. M.; Gileadi, E.; Lipkowski, J.; Schmickler, W.; Trasatti, S. Definition of the Transfer Coefficient in Electrochemistry (IUPAC Recommendations 2014). *Pure Appl. Chem.* **2014,** *86*, 259-262.
(27) Dickinson, E. J. F.; Limon-Petersen, J. G.; Rees, N. V.; Compton, R. G. How Much Supporting Electrolyte Is Required to Make a Cyclic Voltammetry Experiment Quantitatively "Diffusional"? A Theoretical and Experimental Investigation. *J. Phys. Chem. C* **2009,** *113*, 11157-11171.
(28) Ngamchuea, K.; Eloul, S.; Tschulik, K.; Compton, R. G. Advancing from Rules of Thumb: Quantifying the Effects of Small Density Changes in Mass Transport to Electrodes. Understanding Natural Convection. *Anal. Chem.* **2015,** *87*, 7226-7234.
(29) Gavaghan, D. J. How Accurate Is Your Two-Dimensional Numerical Simulation? Part 1. An Introduction. *J. Electroanal. Chem.* **1997,** *420*, 147-158.
(30) Compton, R. G.; Laborda, E.; Ward, K. R. *Understanding Voltammetry: Simulation of Electrode Processes*. Imperial College Press: London, U.K., 2013.
(31) Compton, R. G.; Banks, C. E. *Understanding Voltammetry*. 2nd ed.; Imperial College Press: London, U.K., 2011.
(32) Strem Chemicals Inc., Graphene Nanoplatelets. http://www.strem.com/uploads/resources/documents/graphene_nanoplatelets.pdf (accessed 05 May 2016).
(33) Poon, J.; Batchelor-McAuley, C.; Tschulik, K.; Compton, R. G. Single Graphene Nanoplatelets: Capacitance, Potential of Zero Charge and Diffusion Coefficient. *Chem. Sci.* **2015,** *6*, 2869-2876.
(34) Entigris Inc., *Properties and Characteristics of Graphite*. Entigris Inc.: Billerica, MA, U.S., 2013.
(35) Ellison, J.; Batchelor-McAuley, C.; Tschulik, K.; Compton, R. G. The Use of Cylindrical Micro-Wire Electrodes for Nano-Impact Experiments; Facilitating the Sub-Picomolar Detection of Single Nanoparticles. *Sens. Actuators, B* **2014,** *200*, 47-52.
(36) Batchelor-McAuley, C.; Ellison, J.; Tschulik, K.; Hurst, P. L.; Boldt, R.; Compton, R. G. In Situ Nanoparticle Sizing with Zeptomole Sensitivity. *Analyst* **2015,** *140*, 5048-5054.
(37) Wu, H.; Lin, Q.; Batchelor-McAuley, C.; Goncalves, L. M.; Lima, C. F. R. A. C.; Compton, R. G. Stochastic Detection and Characterisation of Individual Ferrocene Derivative Tagged Graphene Nanoplatelets. *Analyst* **2016,** *141*, 2696-2703.
(38) Laborda, E.; Olmos, J.-M.; Torralba, E.; Molina, A. Application of Voltammetric Techniques at Microelectrodes to the Study of the Chemical Stability of Highly Reactive Species. *Anal. Chem.* **2015,** *87*, 1676-1684.

(39) Laborda, E.; Olmos, J. M.; Martínez-Ortiz, F.; Molina, A. Voltammetric Speciation Studies of Systems Where the Species Diffusivities Differ Significantly. *J. Solid State Electrochem.* **2015,** *19*, 549-561.
(40) Lin, Q.; Li, Q.; Batchelor-McAuley, C.; Compton, R. G. Use of 'Split Waves' for the Measurement of Electrocatalytic Kinetics: Methyl Viologen Mediated Oxygen Reduction on a Boron-Doped Diamond Electrode. *Phys. Chem. Chem. Phys.* **2013,** *15*, 7760-7767.
(41) Kätelhön, E.; Feng, A.; Cheng, W.; Eloul, S.; Batchelor-McAuley, C.; Compton, R. G. Understanding Nano-Impact Current Spikes: Electrochemical Doping of Impacting Nanoparticles. *J. Phys. Chem. C* **2016**.
(42) Wu, H.; Lin, Q.; Batchelor-McAuley, C.; Goncalves, L. M.; Lima, C. F. R. A. C.; Compton, R. G. Stochastic Detection and Characterisation of Individual Ferrocene Derivative Tagged Graphene Nanoplatelets. *Analyst* **2016,** *141*, 2696-2703.
(43) Raoof, J. B.; Ojani, R.; Beitollahi, H.; Hosseinzadeh, R. Electrocatalytic Oxidation and Highly Selective Voltammetric Determination of L-Cysteine at the Surface of a 1-[4-(Ferrocenyl Ethynyl)Phenyl]-1-Ethanone Modified Carbon Paste Electrode. *Anal. Sci.* **2006,** *22*, 1213-1220.

TOC Graphic

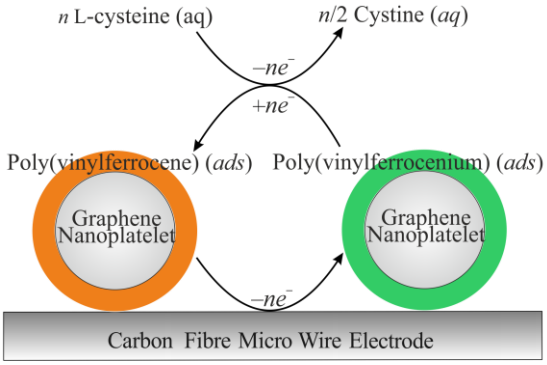
n L-cysteine (aq)
n/2 Cystine (aq)
–ne⁻
+ne⁻
Poly(vinylferrocene) (ads)
Poly(vinylferrocenium) (ads)
Graphene Nanoplatelet
Graphene Nanoplatelet
–ne⁻
Carbon Fibre Micro Wire Electrode